1569618091 7th IEEE International Workshop on Practical Issues in Building Sensor Network Applications 2012 SenseApp 2012, Clearwater, Florida

Follow @grandma: Long-Term Device-Free Localization for Residential Monitoring

Ossi Kaltiokallio
Department of Automation and Systems Technology
Aalto University School of Electrical Engineering
Helsinki, Finland
ossi.kaltiokallio@aalto.fi

Maurizio Bocca and Neal Patwari
Department of Electrical and Computer Engineering
University of Utah
Salt Lake City, Utah, USA
maurizio.bocca@utah.edu, npatwari@ece.utah.edu

***Abstract*—Device-free localization (DFL) enables localizing people by monitoring the changes in the radio frequency (RF) attenuation field of an area where a wireless network is deployed. Notably, this technology does not require people to participate in the localization effort by carrying any electronic device. This paper presents a DFL system for long-term residential monitoring. Due to the daily activities carried out by the people being monitored, the radio signals' propagation patterns change continuously. This would make a system relying only on an initial calibration of the radio environment highly inaccurate in the long run. In this paper, we use an on-line recalibration method that allows the system to adapt to the changes in the radio environment, and then provide accurate position estimates in the long run. A finite-state machine (FSM) defines when the person is located at specific areas-of-interest (AoI) inside the house (e.g. kitchen, bathroom, bed, etc.). Moreover, each time a state transition is triggered, the system tweets the new AoI in a Twitter account. The FSM allows extracting higher level information about the daily routine of the person being monitored, enabling interested parties (e.g. caretakers, relatives) to check that everything is proceeding normally in his life. In the long-term experiment carried out in a real domestic environment, the system was able to accurately and reliably localize the person during his daily activities.**

***Index Terms*—device-free localization, finite-state machine, wireless sensor networks, residential monitoring**

I. Introduction

Device-free localization (DFL) systems locate and track objects (people) by monitoring the changes over time of the received signal strength (RSS) of many static links of a wireless network deployed in the area [1]. These systems, which use the radio channel as the only source of information, do not require people being monitored to carry or wear any electronic device (e.g. mobile phone, RFID tag, low-power transceiver) to participate in the localization task. Potential applications of this technology include surveillance, security and rescue operations, safety systems in industrial areas, and assisted living and elderly care in domestic environments. A DFL system brings several advantages over other traditional technologies, being able to work in cluttered environments and to see through walls [2], smoke and darkness. In addition, this technology does not raise as high privacy concerns as video cameras since identification of people and detailed activity recognition is not possible. Moreover, a DFL system can be composed of low-cost commercial wireless devices which measure RSS. In contrast, ultra-wideband radar devices are also RF-based and can track people through walls, but are prohibitively expensive for many commercial applications.

The different methods used in RSS-based DFL [3], [4], [5], [6], [7] assume that a person affects the propagation of radio signals traveling through the area where he is located. As a consequence, a link's RSS measurements change while a person is located near it, compared to when the person was not near the link. These methods must learn the reference characteristics of the RSS on each link while a person is not nearby to be able to quantify the change when a person is located near the link. However, in cluttered domestic environments, objects of different size, shapes, and material are moved around the house during various daily activities. These movements change the baseline characteristics of RSS on many links. For this reason, the DFL system has to adapt to the changes in the monitored area and recalibrate on-line the reference RSS of the links in order to guarantee a high localization accuracy over an extended period of time. While DFL systems have been deployed for short-term tests, mostly in idealized environments, we are unaware of any long-term tests (more than an hour of measurements) performed in real environments. Besides the traditional challenges associated with enabling reliable communication in long-term wireless network deployments, the DFL system must be able to accurately measure changes in the radio environment without requiring any manual recalibration, reconfiguration, or restarting, even if any particular node fails temporarily. We address these challenges in this paper.

Another challenge to RSS-based DFL systems is that, in a cluttered multipath environment, the statistics of link RSS vary as a function of *fade level* [8]. When a person affects a link in *deep fade* (with lower than average RSS), the RSS fluctuates, with tendency to increase on average. In contrast, for a link in *anti-fade* (with higher than average RSS), the RSS tends to decrease when a person is on the line between the transmitter and receiver. At different frequency channels, a link will be at different fade levels [9]. Thus to improve localization accuracy in challenging residential environments, we exploit the capability of the low-power nodes composing the network to communicate on multiple frequency channels.

This increases the probability that for each link, at least one frequency channel will be in an anti-fade. Channel diversity requires low latency communication among the nodes, while a long-term deployment requires a highly reliable protocol.

When the reference RSS is updated on-line and the monitored person is stationary, with the passing of time the person would slowly stop causing a consistent change in the RSS of the links crossing the area where he is located. Consequently, the estimated attenuation would be close to zero, and therefore the system would assume that the monitored area is empty. In addition, at these times the estimated RSS attenuation images mostly consist of measurement noise. Due to this, the position estimates extracted from the attenuation images move back and forth different areas of the house. To solve these problems, we design a finite-state machine (FSM) capable of keeping track of the person's location when stationary and of filtering out noisy position estimates. The FSM positions the person in one of several pre-defined areas-of-interest (AoI), e.g. kitchen, sofa, bed, bathroom, etc., and allows to extract higher level information about his daily activities. We define state transition rules so as to make the FSM reactive to the person movements while avoiding triggering false state transitions due to noise in the attenuation images.

We present a system which addresses the above challenges and operates in real-time. At each transition of the FSM, the system automatically posts a tweet on the Twitter account associated to the monitored house. The tweet reports include the new AoI and the time of the state transition. The timeline of the tweets posted by the system, which can be made accessible only to authorized individuals, provides a user-friendly and ubiquitous tool allowing interested parties to ensure everything is proceeding normally in the life of the person being monitored. To the best of our knowledge, the system described in this paper is the first to present such long-term, reliable RSS-based DFL of a person during his daily routine in a non-stationary, real-world domestic environment.

II. Related Work

Assisted living and elderly care applications promise a means to improve the quality of life as long as possible for people whose health may be declining. New low-power, minimally-invasive and ubiquitous wireless technologies have paved the way to novel healthcare and medical systems to increase a person's health care outcomes while simultaneously reducing healthcare costs. Several works have proposed various approaches to address degenerative diseases (e.g., diabetes, dementia, etc.) and conditions (posture, fall, body positions and movements during sleep, etc.). These works fall in two categories: in the first, the health and activities of the person being monitored are inferred from data collected by wearable sensors and devices, such as MEMS accelerometers, gyroscopes, microphones, skin conductivity sensors, etc. [10], [11], [12]. Professional athletes often use the same wearable technologies during their training sessions to monitor the stress their bodies undergo during activity or to correct movements' mechanics (e.g., basketball shooting, baseball pitching and batting, etc.) in order to improve their performance [13]. In the second category, sensors and monitoring devices such as cameras, microphones, and radars are scattered in the environment where the person being monitored lives in order to capture patterns representing physical and cognitive health conditions and recognize when these start deviating from the norm [14], [15], [16]. The sensors can also be embedded in the furniture found in the house to monitor the patient during specific activities, as in [17], or to measure the home occupancy time and movement level 24/7 [18].

Our work falls into the latter category – we assume that the person being monitored is not wearing or carrying any electronic device. This is desirable, for example, in the case a person is monitored for possible dementia, because this person may forget to wear sensors, or that such sensors might feel uncomfortable or invasive to some. We target RSS-based DFL as an enabling technology for such elder-care applications. One recent work has run a test of an RSS-based DFL system in an apartment [19] and shown that it can be accurate in room-level localization during a test period. However, the testing period comprised a total of about 5-6 minutes of RSS data. In this work, we target for the first time a long-term deployment of a DFL system in a real domestic environment for residential monitoring purposes. In addition, we aim at sub-meter localization accuracy. We propose methods allowing the system to adapt to the small changes in the radio propagation field caused by the daily activities of the monitored people, such as moving objects of small size around the house, and opening and closing of windows blinds. This self-training ability improves the reliability of the FSM used to position the person in the pre-defined AoIs and avoids triggering false state transitions.

III. System Architecture

A. Hardware and Communication Protocol

We deployed in a 58 square meters apartment 33 Texas Instruments CC2531 USB dongles [20], which are equipped with a low-power, 802.15.4-compliant radio operating in the 2.4 GHz band. We attach the nodes to the wall sockets of the apartment through USB extension cables and power adapters. The nodes are set to transmit at the maximum power ($+4.5$ dBm) over four of the 16 channels defined by the 802.15.4 standard [21]. To collect RSS measurements, we use a multi-channel, TDMA protocol in which each transmitted packet contains the ID of the transmitting node and the most recent RSS measurements of the packets received from the other nodes. When a packet is dropped, the next sensor in the sequence transmits after a back-off time, thus ensuring the networks tolerance to packet drops. At the end of a transmission cycle, the nodes switch synchronously to the next frequency channel in sequence. To avoid the interference generated by coexisting Wi-Fi networks (more than ten found belonging to residents of the neighboring apartments), which would increase the floor noise level of the RSS measurements [22], we selected to use interference-free channels, i.e., channels 15, 20, 25, and 26. A node that overhears all the traffic is

connected to a laptop which processes in real-time the RSS data. On average, the time interval between two consecutive transmissions is 2.9 ms, resulting in a total cycle length of 96 ms. The short transmission interval allows measuring the RSS of each link and channel once every 400 ms.

B. Radio Tomographic Imaging

The goal of an RTI system is to estimate the changes in the attenuation field of the monitored area and to locate the people causing the measured shadowing. The change in RSS between the calibration period and the current instant can be used to estimate the shadowing experienced by each link [3]. However, over long periods of time the propagation patterns of radio signals can change considerably, thus requiring recalibration of the system or adaptation to the changes. Since our system is deployed over an extended period of time, the reference RSS value of each link is calculated using a moving average, which dynamically adjusts to the changing propagation patterns. The sliding average of the RSS measured by the receiver of link *i* at time *k* on channel *c* is:

$$\bar{r}_{i,c}[k] = (1-\alpha)\bar{r}_{i,c}[k-1] + \alpha \cdot r_{i,c}[k], \tag{1}$$

where $\alpha \in [0,1]$ is a smoothing factor defining how fast the mean is updated, and $r_{i,c}[k]$ is the current RSS value. The change at time k in link shadowing is estimated as:

$$S_{i,c} = \bar{r}_{i,c}[k] - r_{i,c}[k]. \tag{2}$$

The change in shadowing on a link is assumed to be a spatial integral of the attenuation field of the monitored area, affected only by voxels of the discretized attenuation field close to the line between the transmitter and receiver. To model this, it is assumed that $S_{i,c}$ is a linear combination of voxel attenuations plus noise:

$$S_{i,c} = \sum_{j=1}^{K} w_{ij} x_{j,c} + n_{i,c}, \tag{3}$$

where $x_{j,c}$ is the change in attenuation in voxel j on channel c, w_{ij} the weight (4) of voxel j for link i, $n_{i,c}$ the noise of link i on channel c, and K the total number of voxels in the estimated image.

The weighting w_{ij} represents how each voxel's attenuation impacts each link. The spatial relationship is modelled geometrically as an ellipse, in which the transmitter and receiver are located at the foci [2], [3], [23], [9]. In this model, voxels j that are overlapped by link i's ellipse have their weight w_{ij} set to a constant, which is inversely proportional to the square root of the Euclidean distance of the nodes. The weight of voxels that are not overlapped are otherwise set to zero. The model can be formulated as:

$$w_{ij} = \frac{1}{\sqrt{d}} \begin{cases} 1 & \text{if } d_{ij}^t + d_{ij}^r < d + \lambda \\ 0 & \text{otherwise} \end{cases}, \tag{4}$$

where d is the distance between the transmitter and receiver, d_{ij}^t and d_{ij}^r are the distances from the center of voxel j to the transmitter and receiver of link i respectively, and λ is the ellipse's excess path length which is used to define its width.

TABLE I
IMAGE RECONSTRUCTION PARAMETERS USED IN THE EXPERIMENTS

Parameter	Value	Description
p	0.2	Pixel width [m]
λ	0.1	Excess path length of weighting ellipse [m]
σ_x	0.2236	Voxels standard deviation [dB]
σ_N	3.1623	Noise standard deviation [dB]
δ_c	4	Decorrelation distance [m]
n_c	2	Number of used channels
α	0.01	Smoothing factor

In [9], it is shown that the accuracy of RTI can be consistently improved by using channel diversity. In this paper, as in [9], we use the fade level as a criterium to select which specific channel's measurements should be used for RTI. In this work, we estimate the fade level of each channel from $\bar{r}_{i,c}$ measured during an initial calibration period. A link is said to be in a deeper fade on channel c_1 then on c_2 if $\bar{r}_{i,c_1} < \bar{r}_{i,c_2}$. In RTI, we consider only the n_c channels whose fade levels are the highest. The average shadowing y_i measured on the n_c most highest fade levels of link i can now be computed as follows:

$$y_i = \frac{1}{n_c} \sum_{c \in \mathcal{F}_i} S_{i,c}, \tag{5}$$

where $\mathcal{F}_i$ is a set of size n_c including the n_c channels with the highest $\bar{r}_{i,c}$. It is to be noted that if $n_c < N$ where N is the total number of used channels, then generally for links i and j, $\mathcal{F}_i \neq \mathcal{F}_j$. In future work, we will include estimating the channels' fade level on-line to gurantee that the best channels for RTI are used at all times.

When all the links of the RF sensor network are considered, the attenuation field can now be modeled as:

$$\mathbf{y} = \mathbf{W}\mathbf{x} + \mathbf{n}, \tag{6}$$

where $\mathbf{y} = [y_1, \ldots, y_L]^T$ is the average change in RSS and $\mathbf{n} = [n_1, \ldots, n_L]^T$ is the measurement noise on the n_c channels, $\mathbf{x} = [x_1, \ldots, x_K]^T$ is the attenuation field to be estimated, and $\mathbf{W}$ is the weight matrix of size $L \times K$ defined in (4). The linear model for shadowing loss is based on the works presented in [3], [24], [25].

Estimating the image vector $\mathbf{x}$ from the link measurements $\mathbf{y}$ is an ill-posed inverse problem, thus regularization is required. To form the image, a regularized least-squares approach [24], [23], [9] is used:

$$\hat{\mathbf{x}} = \mathbf{\Pi}\mathbf{y}, \quad \mathbf{\Pi} = \left(\mathbf{W}^T\mathbf{W} + \mathbf{C}_x^{-1}\sigma_N^2\right)^{-1}\mathbf{W}^T, \tag{7}$$

where σ_N^2 is the noise variance. The a priori covariance matrix $\mathbf{C}_x$ is calculated by using an exponential spatial decay:

$$[\mathbf{C}_x]_{jh} = \sigma_x^2 e^{-d_{jh}/\delta_c}, \tag{8}$$

where d_{jh} is the Euclidean distance of voxels j and h, σ_x^2 is the variance of voxel attenuation, and δ_c is a correlation coefficient. The linear transformation $\mathbf{\Pi}$ can be calculated beforehand, enabling real-time image reconstruction. The image reconstruction parameters used in the experiments of Section IV are listed in Table I.

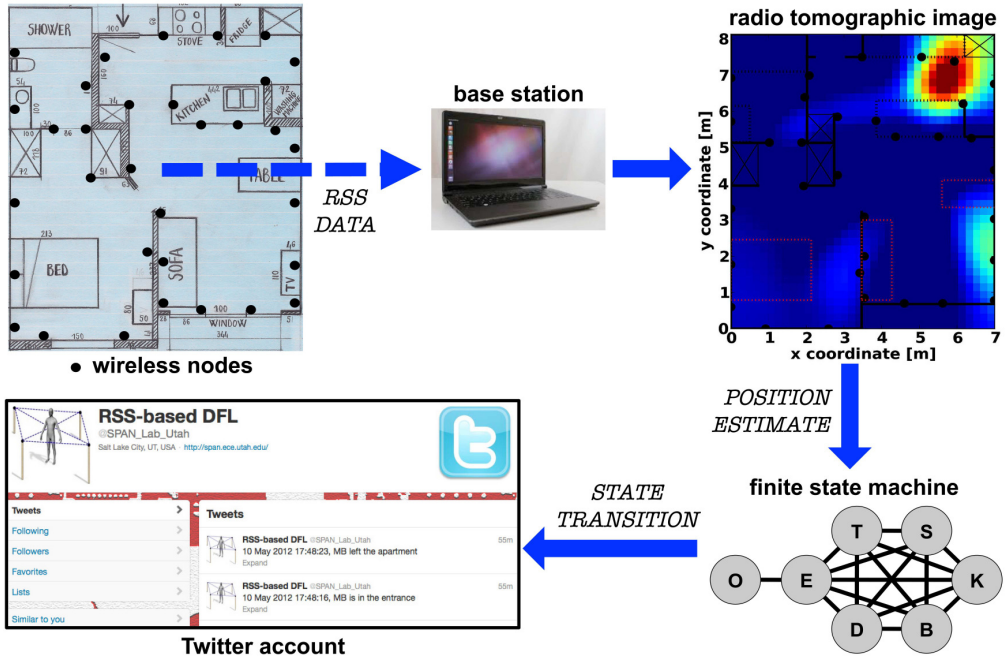

Fig. 1. The system architecture: the RSS measurements collected in the network are processed in real-time to produce radio tomographic images and estimate the current position of the person. This estimate is passed as an input to the finite-state machine, which eventually triggers state transitions. A tweet is posted on the Internet each time a new event (change of AoI) is detected.

C. State Machine

When the monitored person is stationary, the measured attenuation approaches zero over time, since the reference RSS is updated using the moving average (1). Due to this, other methods are needed to keep track of the person when stationary. A finite-state machine (FSM) is designed to define in real-time in which AoI the person is located at and to trigger state transitions in correspondence to his movements. We divide the apartment into six areas-of-interest (AoI), i.e. *E=entrance*, *K=kitchen*, *T=table*, *S=sofa*, *D=bed* and *B=bathroom* as shown in Fig. 2(a), and assign a state to each of them. Another state is added to consider the condition in which the apartment is empty. The states, apart the *O=empty* state, are fully connected, as shown in Fig. 1 and a transition between any two of these states is possible. We set the FSM to be allowed to switch from the state empty exclusively to the state entrance. Similarly, the entrance state is the only one allowed to switch to the state empty. In the following, the state transition conditions between the fully connected part $l \in \{E, T, S, K, B, D\}$ of the FSM is explained in detail followed by the rules that must be fulfilled to switch to the state empty.

The FSM receives as an input the current position which can be estimated by finding the voxel j of the RTI image that has the maximum value:

$$j = \arg\max_{N} \hat{\mathbf{x}}. \tag{9}$$

The position estimate is therefore $\hat{z} = z_j$. At each time instant, we find the AoI A_l to which the position estimate belongs to, $\hat{z} \in A_l$, where $l \in \{E, T, S, K, B, D\}$. A positive counter variable h_l ($\forall\ l : h_l \geq 0$) is incremented by one if $\hat{z} \in A_l$. Otherwise, it is decremented by one if $h_l \neq 0$. A state transition is triggered if the following conditions are met:

TABLE II
PARAMETERS OF THE FINITE-STATE MACHINE USED IN THE EXPERIMENT

Parameter	Value	Description
T_h	20	Number of required $\hat{z} \in A_l$
$T_l \quad l = O$	0.05	Initial value for state *empty*
$T_l \quad l \neq O$	0.1	Initial value for *other* states
n_x	20	Number of samples to calculate median
β	0.25	Smoothing factor

1) *Minimum Duration*: Typically, the position estimates are accurate and could be used on their own to trigger state transitions. However, inaccurate position estimates would cause false transitions if the system would trigger transitions based only on a single one. Thus, to increase the robustness of the system, multiple position estimates have to locate in the same AoI before triggering the state transition. The state transition is triggered when the counter h_l exceeds a pre-defined threshold T_h, i.e., $h_l \geq T_h$. This condition defines the reactivity of the state machine. Small values of T_h cause the state machine to quickly trigger a transition when an AoI is entered, increasing the probability of false transitions, whereas large values improve the robustness of the system, but also the probability of reacting slowly to real movements of the person.

(a) (b) (c)

Fig. 2. In (a), the six identified AoI (E=entrance, K=kitchen, T=table, S=sofa, D=bed, B=bathroom), in (b) the detail of a USB dongle plugged into a wall socket, in (c) the apartment used for the deployment.

2) *Expiration Time*: The counter h_l used for the first condition can increment over a long time period, eventually triggering a false state transition. To avoid this, an expiration timer is used. Whenever the current position estimate belongs to a new AoI, a timer $t_l = 3T_h$ is started. In order for the FSM to trigger a transition, the other two conditions have to be fulfilled before the timer expires, i.e., $t_l \geq 0$.
3) *Image Intensity*: In this paper, we use image intensity as a synonym for the voxel j of the RTI image that has the maximum value, i.e., $\hat{x}_j$. High image intensity values are recorded when multiple links crossing the person's location measure attenuation simultaneously. On the other hand, low values are measured when the monitored area is not occupied or when the person is stationary for a long period of time. A median $\tilde{m}$ is calculated from the last n_x image intensities. The median value has to exceed a threshold for this condition to be valid, i.e. $\tilde{m} \geq 0.5T_l$, where $T_l = (1-\beta)T_{l,k-1} + \beta \cdot \hat{x}_j$. In the on-line threshold update, $k-1$ is the time when the previous transition to state l was triggered, and $\beta \in [0,1]$ is a smoothing factor. This condition filters spurious state transitions by neglecting images with low intensity, i.e. $\hat{x}_j \approx 0$.

The state transition from the state entrance to empty is exclusive and the state transition condition differs from the other conditions. The transition is made only when $\tilde{m} \leq 2T_l$, *i.e.* the image intensity is low. In addition, conditions 1 and 2 must be fulfilled. The FSM parameters are derived using experimental data and the ones used in the experiments of Section IV are listed in Table II.

When a state transition is triggered, the current state s is set to s_l, the counter h_l is reset to zero, and a tweet is posted. However, if the current state is the same as the previous one, the transition is not triggered. The adaptive thresholding method implemented in the FSM guarantees real-time reactivity to the movements of the person and filters out false transitions that can be triggered by particular events, such as wind blowing through the windows and moving the curtains.

The tweets are posted on the Internet at [26] each time the FSM triggers a state transition. The tweets consist of time of the event and the new AoI occupied by the person. The tweets can be made accessible to authorized individuals (*followers*), such as relatives or caretakers of the person being monitored. In this paper, the account is made accessible to everyone. The overall architecture of the system is shown in Fig. 1.

IV. Experimental results

In this section, we evaluate the performance of the system described in Section III. We deploy the network in a typical single floor, single bedroom apartment, shown in Fig. 2(c), for one week. During this time, we do not recalibrate the reference RSS or restart the system. Our goal is to prove that the system can accurately trigger the state transitions among the AoI (Fig. 2(a)) and adapt to the changing environment over an extended period of time.

Before the long-term deployment is started, we estimate the localization accuracy of the system. In the experiment, a person is standing still at one of the 14 known positions for a predetermined time, after which the person moves to the next location. The positions are chosen to cover all areas of the apartment and each position is visited two times. The position estimates are obtained from the RTI images as described in Section III and the root-mean-squared error (RMSE) of the position estimates is 0.23 m. The true and estimated positions of the experiment are shown in Fig. 4. Although we have not done so, the accuracy is such that the system could be designed to have more AoI and to recognize more specific activities such as: cooking by the stove, washing laundry and selecting clothes from the closet.

To validate the capability of the system to correctly identify the AoI in which the person is in and to correctly switch among the states, we conduct a two hours test during which we record the correct sequence of visited AoI and the precise instants of transition. During the test, each AoI is visited

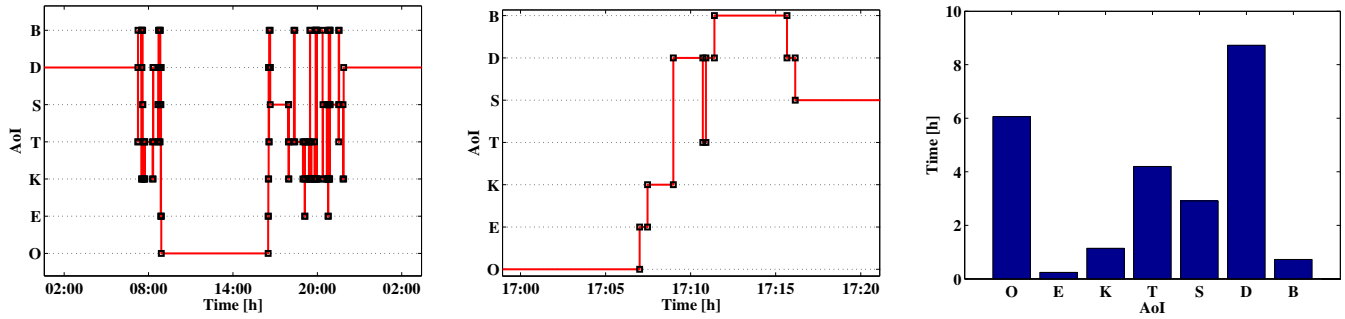

(a) (b) (c)

Fig. 3. In (a) the daily activities (Wednesday-Thursday) of the test person and in (b) a 20 minute time window when the person arrives home from work. In (c) the average time spent on each activity per day over the one week test period.

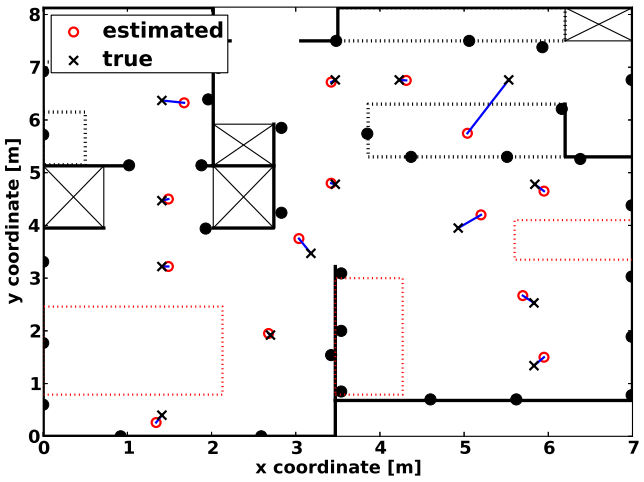

Fig. 4. The localization accuracy of the system is tested in 14 different positions marked in the figure with black crosses. The position estimates calculated from the RTI images are illustrated with red circles. The RMSE in the 14 different positions is 0.23 m.

multiple times, for a total of 60 state transitions. Also, to better simulate the *real* life, we ask the person being monitored to perform an activity in each AoI (e.g. wash his hands, open and close the fridge, move an object, etc.) that would change the radio signal propagation patterns in the area. The correct sequence of transitions and their time stamps are then compared to the tweets posted by the system. During this test, the system correctly detected all of the state transitions and generated no false transitions. However, during the one week deployment it was noticed that the system triggered occasionally false transitions. Despite the false transitions, the system was capable of recovering to its true state after some time or when the person visited another AoI. The false transitions were caused by neighbours movement outside the apartment.

From the higher level information extracted over a long period of time it is possible to analyze the daily routines of the person, as shown in Fig. 3. In (a), the activities of the monitored person over a single day are shown. From this figure, it can be pointed out when, e.g., the person wakes up, relaxes on the sofa, leaves the apartment or returns home from work as shown in (b). In (c), the average time spent per day in each AoI is shown. The data are averaged over the whole week, including working day and week-end.

For example in an assisted living scenario, if the caretakers would be familiar with the expected daily routine of the monitored person, they could interpret the daily activities of the person to estimate the health or condition of the patient. For example, if the person being monitored wakes up late in the morning, does not spend sufficient time in the kitchen, and does not leave the apartment as expected, one could reasonably assume that the person might be depressed or sick. These signs would indicate that the person should be visited soon so that a closer examination could be made.

The system is able to produce accurate attenuation images throughout the entire length of the test, as shown in Fig. 5. Figures (a)-(e) show attenuation images obtained by applying the moving average (1). With this method, the system is capable of adapting to the varying environment. When the radio signal propagation patterns change, due to e.g. opening and closing of windows or movements of objects, the system dynamically adjusts the reference RSS of the lines traveling across the monitored area. On the other hand, a system that would use as reference RSS only the measurements collected during an initial calibration phase would not be able to adapt to the changes of the propagation patterns caused by the daily activities of the person being monitored. Figures (f)-(j) show how in this case the noise of the images produced by the system would quickly increase to the point of making a reliable estimate of the person's location impossible.

V. Lessons Learned

The long-term deployment of the RSS-based DFL system in a real domestic environment has provided the opportunity to gain useful insights about this measurement modality. In a first deployment, we had positioned the nodes so to have a homogeneous density of wireless links over the monitored area. However, in few key areas of the apartment the lo-

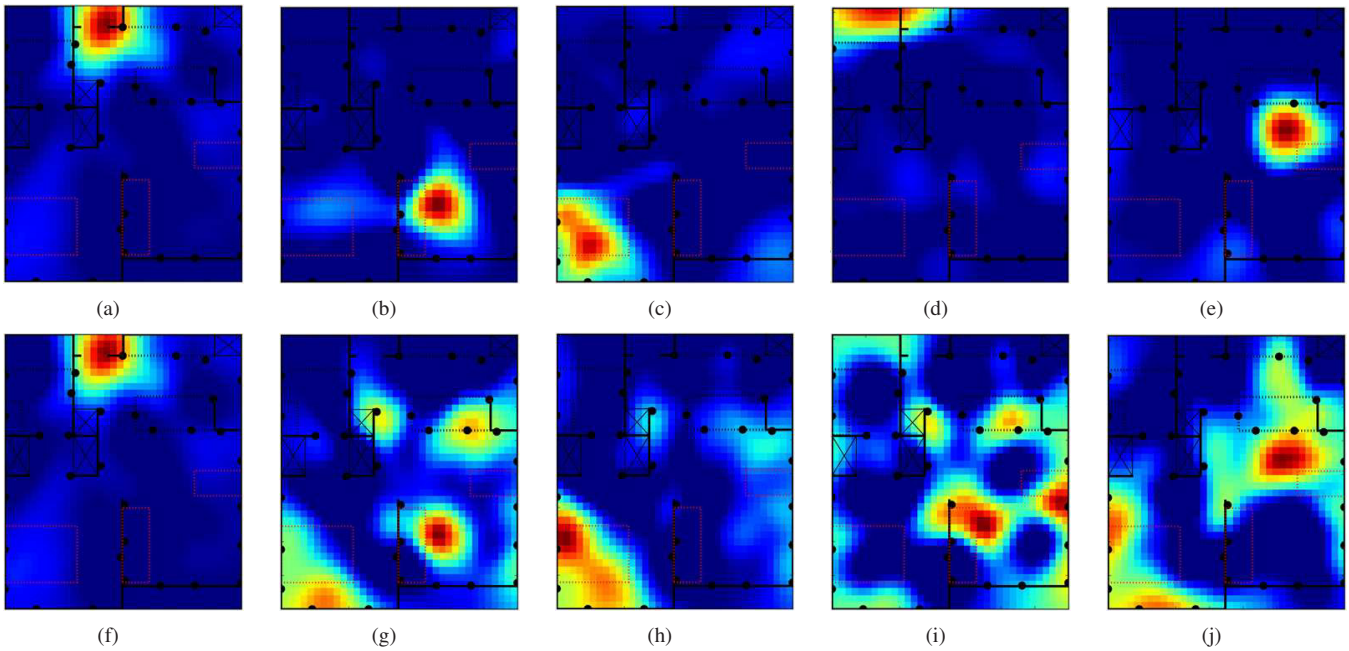

Fig. 5. Attenuation images obtained when the reference RSS is calculated by applying the moving average (a)-(e) and when it is not updated after an initial calibration (f)-(j). Starting from the left, the images are plotted over one day in 6 hours intervals : in (a) and (f), the person is located at the entrance, in (b) and (g) on the sofa, in (c) and (h) in bed, in (d) and (i) in the bathroom and in (e) and (j) by the table. When the reference RSS is not updated, the images become noisy over time due to changes in the radio signal propagation patterns, eventually providing wrong position estimates, as in (i).

calization accuracy provided by the system was poor. By observing the raw RSS measurements traveling across these challenging areas, we were able to identify which nodes had been positioned in spots that were particularly hostile for the propagation of the radio signals, e.g. leaning against a large marble counter found in the kitchen. Our solution was to distance the antennas of the nodes by few centimeters from this marble surface and also from the walls of the apartment. After this adjustment, the system was able to accurately localize the person throughout the entire monitored area.

One of the main concerns in deploying a RSS-based DFL system in a real environment is the number of nodes required to provide a sufficiently accurate localization throughout the monitored area. For this reason, we analyze in simulations the effect of removing nodes from the system, i.e. lowering the number of nodes composing the network. The results are shown in Fig. 6. The simulations are conducted with the same data used to validate the localization accuracy of the system. Removing each number of nodes is simulated 20 times. The removed nodes are selected randomly to validate the RMSE when various nodes do not participate in the localization effort. On average, the RMSE increases as more nodes are removed from the network. The results of the simulations vary considerably when different nodes are removed, indicating that some nodes of the network are more important than others to achieve accurate localization. Moreover, the smallest RMSEs show that accurate positioning can be achieved also with fewer nodes. However, these nodes would need to be positioned at locations that would favor RTI. In addition, by analyzing the

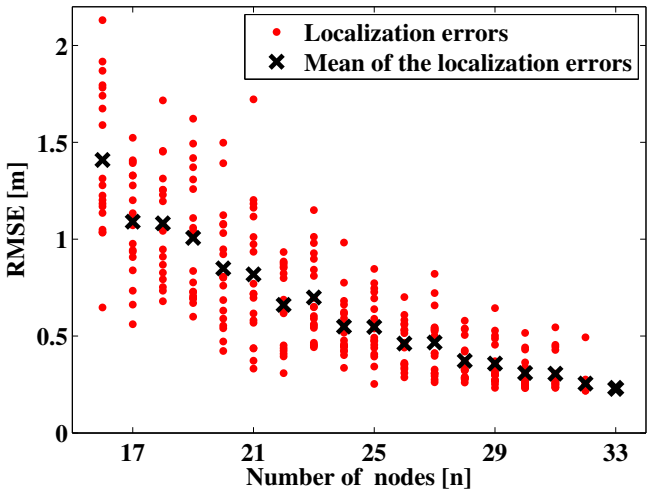

Fig. 6. Results of the simulations in which fewer nodes are used to collect RSS measurements.

results of the simulations we were able to observe that, by removing few particular nodes, higher localization accuracy was achieved compared to a system relying on all the nodes.

While analyzing the RSS measurements collected by the nodes and the overall performance of the system, we were also able to identify few, unexpected sources of variance in the data. For example, due to the limited thickness of the walls separating the apartment from the neighboring ones and the main corridor of the building, the movements of people found in the surrounding apartments and along the corridor affected

the RSS measured by the nodes deployed on the separating walls. On few occasions, we were even able to track the movements of people outside the apartment along the walls. Thus, we had to keep in mind this issue while developing the adaptive thresholding method used in the FSM.

VI. Conclusion

In this paper, we present a RSS-based DFL system for long-term residential monitoring which is capable of accurately localizing in real-time the person being monitored in a real domestic environment over an extended period of time. To achieve these goals, we propose the use of channel diversity and of methods that adapt to the continuous changes in the radio signal propagation patterns due to the daily activities of the monitored person and the non-stationary nature of the environment. Higher-level information is obtained through a FSM which keeps track of the person location when he is stationary and filters out localization estimates which are affected by random noise in the RSS measurements. The capability of the system to provide accurate estimates in the long-term may be exploited in the future for a variety of purposes, such as monitoring the social interactions of people possibly affected by depression, or the level of sedentarity of obese people. The work presented in this paper shows that device-free localization represents an inexpensive and minimally-invasive technology that can improve the quality of life for people whose health may be declining and simultaneously provide a useful support to their caretakers.

Acknowledgments

This work is funded by the Finnish Funding Agency for Technology and Innovation (TEKES). This material is also based upon work supported by the US National Science Foundation grants 0748206 and 1035565. The authors wish to thank Brad Mager for the extensive help in setting up the experiments.

References

[1] N. Patwari and J. Wilson, "RF sensor networks for device-free localization and tracking," *Proceedings of the IEEE*, vol. 98, no. 11, pp. 1961–1973, Nov. 2010.

[2] J. Wilson and N. Patwari, "See through walls: motion tracking using variance-based radio tomography networks," *IEEE Trans. Mobile Computing*, vol. 10, no. 5, pp. 612–621, May 2011, appeared online 23 September 2010.

[3] J. Wilson and N. Patwari, "Radio tomographic imaging with wireless networks," *IEEE Trans. Mobile Computing*, vol. 9, no. 5, pp. 621–632, May 2010, appeared online 8 January 2010.

[4] M. A. Kanso and M. G. Rabbat, "Compressed RF tomography for wireless sensor networks: Centralized and decentralized approaches," in *5th IEEE Intl. Conf. on Distributed Computing in Sensor Systems (DCOSS-09)*, Marina Del Rey, CA, June 2009.

[5] R. K. Martin, C. Anderson, R. W. Thomas, and A. S. King, "Modelling and analysis of radio tomography," in *2011 4th IEEE International Workshop on Computational Advances in Multi-Sensor Adaptive Processing (CAMSAP)*, Dec. 2011.

[6] O. Kaltiokallio and M. Bocca, "Real-time intrusion detection and tracking in indoor environment through distributed rssi processing," in *2011 IEEE 17th Intl. Conf. Embedded and Real-Time Computing Systems and Applications (RTCSA)*, vol. 1, Aug. 2011, pp. 61 –70.

[7] X. Chen, A. Edelstein, Y. Li, M. Coates, M. Rabbat, and M. Aidong, "Sequential Monte Carlo for simultaneous passive device-free tracking and sensor localization using received signal strength measurements," in *ACM/IEEE Information Processing in Sensor Networks (IPSN)*, April 2011.

[8] J. Wilson and N. Patwari, "A fade level skew-Laplace signal strength model for device-free localization with wireless networks," *IEEE Trans. Mobile Computing*, appeared online 12 May 2011.

[9] O. Kaltiokallio, M. Bocca, and N. Patwari, "Enhancing the accuracy of radio tomographic imaging using channel diversity," in *the 9th IEEE International Conference on Mobile Ad hoc and Sensor Systems*, October 2012, to appear.

[10] Q. Li, J. A. Stankovic, M. A. Hanson, A. T. Barth, J. Lach, and G. Zhou, "Accurate, fast fall detection using gyroscopes and accelerometer-derived posture information," in *Proceedings of the 2009 Sixth International Workshop on Wearable and Implantable Body Sensor Networks*, ser. BSN '09. Washington, DC, USA: IEEE Computer Society, 2009, pp. 138–143.

[11] A. T. Barth, B. Boudaoud, J. S. Brantley, S. Chen, C. L. Cunningham, T. Kim, H. C. Powell, Jr., S. A. Ridenour, J. Lach, and B. C. Bennett, "Longitudinal high-fidelity gait analysis with wireless inertial body sensors," in *Wireless Health 2010*, ser. WH '10. New York, NY, USA: ACM, 2010, pp. 192–193.

[12] T. Kim, S. Chen, and J. Lach, "Detecting and preventing forward head posture with wireless inertial body sensor networks," in *Body Sensor Networks (BSN), 2011 International Conference on*, 05/2011 2011, pp. 125 –126.

[13] M. Lapinski, E. Berkson, T. Gill, M. Reinold, and J. A. Paradiso, "A distributed wearable, wireless sensor system for evaluating professional baseball pitchers and batters," in *Proceedings of the 2009 International Symposium on Wearable Computers*, ser. ISWC '09. Washington, DC, USA: IEEE Computer Society, 2009, pp. 131–138.

[14] D. Anderson, J. Keller, M. Skubic, X. Chen, and Z. He, "Recognizing falls from silhouettes," in *Engineering in Medicine and Biology Society, 2006. EMBS '06. 28th Annual International Conference of the IEEE*, 30 2006-sept. 3 2006, pp. 6388 –6391.

[15] L. Liu, M. Popescu, M. Skubic, M. Rantz, T. Yardibi, and P. Cuddihy, "Automatic fall detection based on doppler radar motion signature," in *Pervasive Computing Technologies for Healthcare (PervasiveHealth), 2011 5th International Conference on*, may 2011, pp. 222 –225.

[16] Y. Li, K. C. Ho, and M. Popescu, "A microphone array system for automatic fall detection," *IEEE Trans. Biomed. Engineering*, vol. 59, no. 5, pp. 1291–1301, 2012.

[17] E. Hoque, R. F. Dickerson, and J. A. Stankovic, "Monitoring body positions and movements during sleep using wisps," in *Wireless Health 2010*, ser. WH '10. New York, NY, USA: ACM, 2010, pp. 44–53. [Online]. Available: http://doi.acm.org/10.1145/1921081.1921088

[18] R. F. Dickerson, E. I. Gorlin, and J. A. Stankovic, "Empath: A continuous remote emotional health monitoring system for depressive illness," in *Wireless Health*, San Diego, 10/2011 2011.

[19] C. Xu, B. Firner, Y. Zhang, R. Howard, J. Li, and X. Lin, "Improving RF-based device-free passive localization in cluttered indoor environments through probabilistic classification methods," in *Proc. Information Processing in Sensor Networks (IPSN-2012)*, April 2012, pp. 209–220.

[20] Texas Instruments. A USB-enabled system-on-chip solution for 2.4 GHz IEEE 802.15.4 and ZigBee applications. [Online]. Available: http://www.ti.com/lit/ds/symlink/cc2531.pdf

[21] IEEE 802.15.4 standard technical specs. [Online]. Available: http://www.ieee802.org/15/pub/TG4Expert.html

[22] K. Srinivasan, P. Dutta, A. Tavakoli, and P. Levis, "Understanding the causes of packet delivery success and failure in dense wireless sensor networks," in *SenSys*, 2006, pp. 419–420.

[23] Y. Zhao and N. Patwari, "Noise reduction for variance-based device-free localization and tracking," in *8th IEEE Conference on Sensor, Mesh and Ad Hoc Communications and Networks (SECON'11)*, June 2011.

[24] N. Patwari and P. Agrawal, "Effects of correlated shadowing: Connectivity, localization, and RF tomography," in *IEEE/ACM Int'l Conf. on Information Processing in Sensor Networks (IPSN'08)*, April 2008, pp. 82–93.

[25] P. Agrawal and N. Patwari, "Correlated link shadow fading in multi-hop wireless networks," *IEEE Trans. Wireless Commun.*, vol. 8, no. 8, pp. 4024–4036, Aug. 2009.

[26] SPAN Lab, ECE Department, University of Utah. [Online]. Available: https://twitter.com/#!/SPAN_Lab_Utah